Secretagogin-dependent matrix metalloprotease-2 release from neurons regulates neuroblast migration

János Hanics[a,b,1], Edit Szodorai[c,d,1], Giuseppe Tortoriello[e,2], Katarzyna Malenczyk[c,e], Erik Keimpema[c], Gert Lubec[d], Zsófia Hevesi[a,b], Mirjam I. Lutz[f], Márk Kozsurek[b], Zita Puskár[b], Zsuzsanna E. Tóth[b], Ludwig Wagner[g], Gábor G. Kovács[f], Tomas G. M. Hökfelt[e,3], Tibor Harkany[c,e], and Alán Alpár[a,b,3]

[a]MTA-SE NAP B Research Group of Experimental Neuroanatomy and Developmental Biology, Hungarian Academy of Sciences, H-1051 Budapest, Hungary; [b]Department of Anatomy, Histology, and Embryology, Semmelweis University, H-1085 Budapest, Hungary; [c]Department of Molecular Neurosciences, Center for Brain Research, Medical University of Vienna, A-1090 Vienna, Austria; [d]Department of Pharmaceutical Chemistry, Faculty of Life Sciences, University of Vienna, A-1090 Vienna, Austria; [e]Department of Neuroscience, Karolinska Institutet, SE-171 77 Stockholm, Sweden, [f]Institute of Neurology, Medical University of Vienna, A-1090 Vienna, Austria, and [g]Department of Internal Medicine III, Medical University of Vienna, A-1090 Vienna, Austria

Contributed by Tomas G. M. Hökfelt, January 19, 2017 (sent for review September 15, 2016; reviewed by Leszek Kaczmarek, George Kuhn, and Armen Saghatelyan)

The rostral migratory stream (RMS) is viewed as a glia-enriched conduit of forward-migrating neuroblasts in which chemorepulsive signals control the pace of forward migration. Here we demonstrate the existence of a scaffold of neurons that receive synaptic inputs within the rat, mouse, and human fetal RMS equivalents. These neurons express secretagogin, a Ca^{2+}-sensor protein, to execute an annexin V-dependent externalization of matrix metalloprotease-2 (MMP-2) for reconfiguring the extracellular matrix locally. Mouse genetics combined with pharmacological probing in vivo and in vitro demonstrate that MMP-2 externalization occurs on demand and that its loss slows neuroblast migration. Loss of function is particularly remarkable upon injury to the olfactory bulb. Cumulatively, we identify a signaling cascade that provokes structural remodeling of the RMS through recruitment of MMP-2 by a previously unrecognized neuronal constituent. Given the life-long presence of secretagogin-containing neurons in human, this mechanism might be exploited for therapeutic benefit in rescue strategies.

human fetus | calcium-binding protein | cell motility | restorative strategy | olfactory system

The subventricular zone of adult rodents and its human fetal equivalent (1) generate neuroblasts that migrate through the rostral migratory stream (RMS) to supply the olfactory bulb with new neurons (2). Tangential neuroblast migration in the RMS is regulated by various environmental factors including growth factors (3–10), ephrins (11), and cell adhesion-related cues (12–14). Many of these regulatory events are executed through direct intercellular interactions: Chain-migrating neuroblasts move in contact with each other (15), and neuron–glia communication shapes the journey of newborn cells toward the olfactory bulb (16, 17). In particular, astrocytes can vector neuroblast movement by secreting netrin (18) and VGEF (19, 20) and regulate the speed of migration by releasing GABA (21, 22) while actively reconfiguring their own network in response to neuroblast-derived signals through the Slit/Robo machinery (16).

Brain extracellular matrix is a juxtacellular scaffold that defines the microenvironmental arrangements surrounding each cell. Extracellular matrix components were earlier implicated in neuroblast migration: Tenascin-R can mediate activity-dependent neuroblast recruitment, (23) and hyaluronan and its receptor, Rhamm, driving hyaluronan-mediated motility, are selectively expressed in the adult RMS (24). Notably, members of the matrix metalloproteinase (MMP) family are recognized as critical for restructuring the extracellular matrix by cleaving all its components (25, 26). However, MMP activity and efficacy in neurogenic niches were studied chiefly in the early postnatal nervous system (12), during axonal growth, and upon cancer cell invasion (27–29) with pathologically increased proliferative capacity. In the RMS, MMP inhibitors reduce the rate of neuroblast migration in young mice, but chain migration remains unaffected in the adult (12). Here, MMP activity was shown to surround chain-migrating neuroblasts (12). However, the cellular source of any specific MMP family member, the molecular determinants of its liberation, and its evolutionary conservation between rodents and human remain unknown.

Ca^{2+} sensor proteins undergo conformational changes upon Ca^{2+} binding, which then triggers intermolecular interactions with downstream effectors to regulate activity-dependent release or signaling events (30, 31). Secretagogin is one such protein (32) with a phylogenetically conserved distribution in vertebrates (33, 34). Explored first in pancreatic beta cells, secretagogin was shown to interact with the SNARE machinery (32). Similarly, secretagogin's proteome-wide interactions posit a role in neuropeptide release from hypothalamic neurons (35).

Here, we identify a population of neurons that express secretagogin within the adult murine RMS to control MMP2, but not MMP9, externalization through annexin V recruitment. This focal and "on-demand" MMP2 release affects only motile neuroblasts but is unlikely to mobilize the source cells themselves. Based on histochemical analysis advancing to the ultrastructural level in rodent and human fetal brains, we suggest that secretagogin-containing neurons are a cell population in the RMS that form a scaffold around migrating neuroblasts. By developing in situ zymography

Significance

Persisting proliferative capacity and regeneration in the adult brain are confined to a minority of regions. In the murine brain, the olfactory system is supplied by thousands of newly born neuroblasts daily to support sensory plasticity. Here, we reveal a neuronal scaffold that resides within and alongside this migratory route [termed the "rostral migratory stream" (RMS)] to guide forward migration of newly born neuroblasts. These neurons can externalize the enzyme matrix metalloprotease-2 to loosen the extracellular matrix, thus producing permissive corridors for migrating neuroblasts. This mechanism is likely phylogenetically conserved because it exists in the RMS equivalent in human fetal brains. This inducible mechanism might be pharmacologically targeted for therapeutic benefit.

Author contributions: J.H., E.S., T.G.M.H., T.H., and A.A. designed research; J.H., E.S., Z.H., M.L., M.K., Z.P., Z.E.T., and A.A. performed research; L.W. and G.G.K. contributed new reagents/analytic tools; J.H., E.S., G.T., K.M., E.K., G.L., T.H., and A.A. analyzed data; and T.H. and A.A. wrote the paper.

Reviewers: L.K., Nencki Institute; G.K., University of Gothenburg; and A.S., Centre de Recherche de l'Institut Universitaire en Santé Mentale de Québec.

The authors declare no conflict of interest.

[1]J.H. and E.S. contributed equally to this work.

[2]Present address: Thermo Fisher Scientific, Life Sciences Solutions Group, 20900 Monza, Italy.

[3]To whom correspondence may be addressed. Email: tomas.hokfelt@ki.se or alpar.alan@med.semmelweis-univ.hu.

This article contains supporting information online at www.pnas.org/lookup/suppl/doi:10.1073/pnas.1700662114/-/DCSupplemental.

and combining this technique with mass spectrometry, we show that secretagogin-containing neurons are the foci of MMP-2 release in the rodent brain. We then generated secretagogin knockout mice and performed in vivo and in vitro gene silencing to dissect molecular interactions among secretagogin, annexin V, and MMP-2. Cumulatively, we identified a hitherto undescribed neuronal contingent and its selective MMP-2–externalization mechanism that controls neuroblast migration by restructuring the extracellular matrix, a mechanism conserved between rodents and human.

Results

Secretagogin-Expressing Neurons Form a Scaffold in the Rodent RMS. Cellular interactions in the RMS are mandatory for the coordinated chain migration of neuroblasts toward the olfactory bulb (3, 4, 6, 16). In rodents, adult-born neurons migrate in permissive corridors ("tunnels") established by a complex network of astrocytes (2). Neuron–glia communication is pivotal in this process, together with the active participation of neuroblasts transforming the astrocytic tunnel (36). However, the mechanisms of communication between newborn neurons and a contingent of nonastroglial cells resident in the RMS remain unexplored. Here, we show that secretagogin labels a distinct subset of bipolar cells (Fig. 1 A_1–A_3) primarily populating the outer region of the adult rat RMS (Fig. 1 A_1–A_3) and significantly outnumbering the cells in its inner compartment ("axis") (Fig. 1A_2). In accord with recent human terminology (37), this localization pattern allows an onion skin-like cellular matrix suited to direct neuroblasts toward the olfactory bulb. Secretagogin immunoreactivity was detected in both somata (Fig. 1 A_1–A_3) and processes (Fig. 1A_2). When the subcellular compartmentalization of secretagogin was analyzed at the ultrastructural level, particularly in cells contacting chain-migrating neuroblasts (Fig. 1B), secretagogin typically was detected in processes (Fig. 1B_1 and Fig. S1E), many of which emanated perpendicular to the axis of the RMS (Fig. 1B_2). Secretagogin immunoreactivity often was closely associated with the membrane of the endoplasmic reticulum (Fig. S1 A and A_1) and mitochondria (Fig. S1B). In some cases, secretagogin$^+$ focal accumulations were selectively seen in the RMS, which surrounded dendrite-like profiles (Fig. S1 F, F_1, and G), suggesting focal signaling events through protein recruitment.

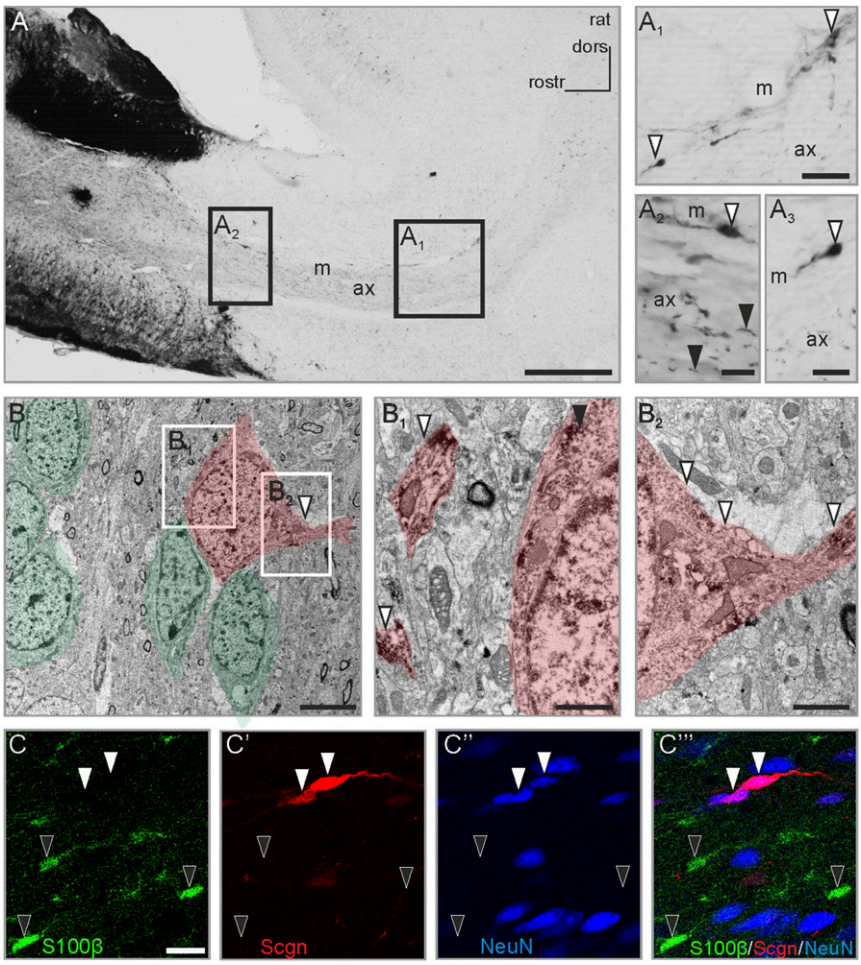

Fig. 1. The presence and compartmentalization of secretagogin in rat RMS neurons. (A–A_3) Secretagogin$^+$ cells populate the rat RMS. In addition to somatic labeling (open arrowheads in A_1–A_3) a large number of individual processes were identified in the center of the middle domain of the stream (black arrowheads in A_2; also see Fig. S1E). Additionally, secretagogin$^+$ cells often delineated the border of the RMS with their processes extended bipolarly (open arrowheads in A_1 and A_3). (B) Ultrastructural analysis identified secretagogin$^+$ cells in close contact with chain-migrating neurons with secretagogin expression detectable both in the soma (black arrowhead in B_1 and in processes arranged in parallel (open arrowheads in B_1) or transversally (open arrowheads in B_2). Chain-migrating neuronblasts and secretagogin$^+$ cells are semitransparently color-coded in green and red, respectively. (C–C''') Secretagogin$^+$ cells were invariably immunonegative for the gilal marker S100β (black arrowheads in C–C''') but were immunopositive for the neuron marker NeuN (white arrowheads in C'–C'''). ax, axis of RMS; dors, dorsal; m, marginal zone of RMS; rostr, rostral; Scgn, secretagogin. (Scale bars: 500 μm in A, 30 μm in A_1 and A_2; 20 μm in A_3; 15 μm in C–C'''; 10 μm in A_2 and A_4; 5 μm in B; 2 μm in B_2; and 1 μm in B_1.)

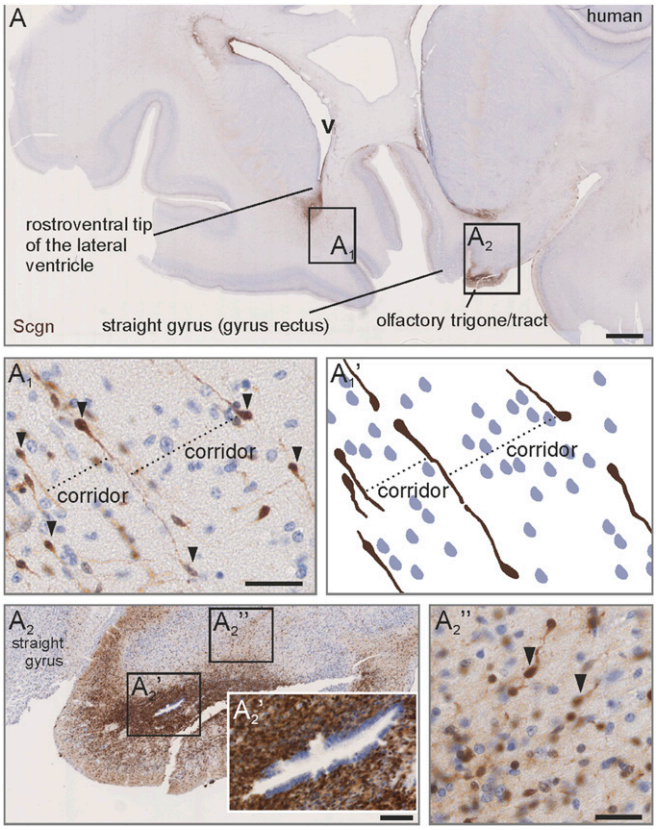

Fig. 2. Secretagogin$^+$ neurons outline a ventriculo-olfactory stream in human fetus. (*A–A1′*) Secretagogin$^+$ neurons were concentrated at the rostroventral tip of the lateral ventricle (*A1*) and emanated in parallel strings ventrally forming corridors (*A1* and *A1′*). The olfactory trigone harbored a high density of secretagogin$^+$ neurons (*A2*), which typically were concentrated around a ventricle-like space surrounded by ependymal cells (*A2′*). Bipolar secretagogin$^+$ neurons formed a cap-shaped region dorsal to the olfactory trigone which pointed toward the ventral pole of the lateral ventricle (*A2″*). Images in *A* and *A2* were acquired using the tile-and-stitch function. v, ventricle. (Scale bars: 1,000 μm in *A*; 200 μm in *A2*; 40 μm in *A1′*, *A2′*, and *A2″*.)

Secretagogin$^+$ cells were negative for neural/glial antigen 2 (NG2 proteoglycan) (Fig. S1 *I*, *I2*, and *I2′*), S100 Ca^{2+}-binding protein B (S100B) (Fig. 1 *C* and *C′* and Fig. S1 *H–H2*), and the microtubule destabilizing protein stathmin-2 (Fig. S1 *I*, *I1*, and *I1′*) typically present in motile neurite tips (38). In contrast, secretagogin$^+$ cells expressed the neuronal nuclear antigen NeuN (Fig. 1 *C–C″*), thus qualifying as bona fide differentiated neurons. Secretagogin$^+$ neurons were positioned with no clear association to local microvessels in either early postnatal or adult rats (Fig. S1 *J–J4″*). Recent studies show that mature neurons establish synapses in the RMS (37, 39), an observation corroborated by the presence of secretagogin in the postsynaptic compartment (Fig. S1 *C* and *D*). Taking these findings together, we suggest that mature neurons might reside in the murine RMS with a spatial configuration aimed at modulating chain migration.

Secretagogin$^+$ Neurons in the Human Fetal Lateral Ventricle and Olfactory Tract. Many mammals retain the ability to generate neurons in adulthood (2, 15, 40–43). In humans, migratory cell streams leaving the subventricular zone cease to exist by 18 mo postpartum (1). Before this time, the infant human subventricular zone and RMS equivalent contain a pool of forward-migrating neuroblasts (1) with their uninterrupted stream connecting the ventral tip of the subventricular zone with the olfactory peduncle (1). By analyzing third-trimester human fetal brains, we find secretagogin$^+$ bipolar cells at the rostroventral pole of the lateral ventricle (Fig. 2 *A* and *A1*). These cells establish a palisade-like parcellated structure that extends toward the base of the brain (Fig. 2 *A1* and *A1′*). By exploiting oblique sectioning, which also includes the proximal domain of the contralateral olfactory tract (Fig. 2*A*), we showed dense secretagogin immunoreactivity (Fig. 2*A2*) with most cells concentrated around the olfactory ventricle (a ventricular space lined by ependymal cells) (Fig. 2*A2′*). A cap-shaped condensation of secretagogin$^+$ neurons was seen dorsal to the olfactory trigone/tract (Fig. 2*A2″*) that retained clear organization through parallel and equally spaced neurons (Fig. 2*A2″*). Considering that all other cells, shown by nuclear staining resided between secretagogin$^+$ "guide" neurons and along their processes (Fig. 2 *A1* and *A2″*), we hypothesize that this cell contingent might be functionally significant in organizing the human fetal RMS equivalent.

Slow Turnover of Secretagogin$^+$ Resident Neurons. Chain-migrating neuroblasts arise from the ventricular wall of adult rat and mouse to enter the RMS (44). Comparative neuroanatomical studies in avians show that secretagogin$^+$ neurons densely populate the rostroventral domain of the lateral ventricle (34). Using BrdU in rats, we labeled newly born neuroblasts at the ventricular wall (Fig. 3 *A* and *B*). Secretagogin$^+$ neurons were BrdU$^-$ and surrounded the doublecortin (DCX)$^+$/BrdU$^+$ migrating neuroblasts (Fig. 3 *B*, *C*, and *D2*), thus producing a tunnel-like demarcation (Fig. 3 *B–D1*). This cellular arrangement extended into the adjacent, proximal part of the RMS (Fig. 3 *E–E1′*), reinforcing the notion that slow-turnover secretagogin$^+$ neurons could be ideally positioned to direct the migration of neuroblasts.

RMS Injury Increases the Number of Secretagogin$^+$ Neurons. After unilateral surgical removal of the olfactory bulb, the subventricular zone and RMS persist and enlarge (43). We hypothesized that their increased size and cell number (43) could affect the number of secretagogin$^+$ neurons, particularly if increased contingents of neuroblasts migrate toward the site of injury. Secretagogin expression significantly increased in the ipsilateral RMS 15 d after bulbectomy throughout the cranio-caudal extension of the RMS (Fig. 4 *A–E*). In addition to a primary increase in the outer regions of the RMS (Fig. 4 *C2*, *D*, and *E*), secretagogin$^+$ neurons were seen with increasing frequency in the RMS axis (Fig. 4 *B′–B‴*).

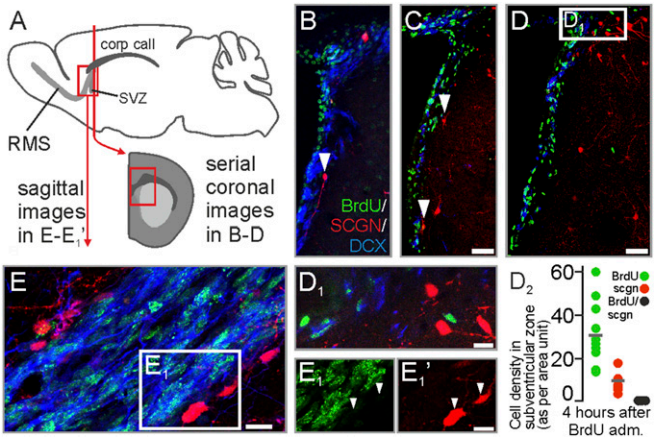

Fig. 3. Secretagogin$^+$ cells in the subventricular zone region and on entry into the RMS. (*A*) Schema of tissue sampling. (*B–D2*) Coronal sections. BrdU$^+$ neuroblasts in the subventricular zone were demarcated toward the neighboring striatum by secretagogin$^+$/BrdU$^-$ neurons. (*E–E1′*) Saggital sections. BrdU$^+$ neuroblasts in the most proximal part of the RMS are demarcated by secretagogin$^+$ neurons (white arrowheads in *E1* and *E1′*). med, medial. (Scale bars: 80 μm in *C* and *D*; 10 μm in *D1*, *E*, and *E1′*.)

This increased frequency was confirmed by quantitative immunohistochemistry (Fig. 4 *F*–*F*″) showing that secretagogin$^+$ neurons retained their native distribution irrespective of bulbectomy (Fig. 4*F*″ and Table S1). Our domain- and region-specific analysis revealed an up to eightfold increase in secretagogin$^+$ neurons in bulbectomized animals as compared with sham-lesioned controls (Fig. 4*F*″). These data together with secretagogin cells remaining BrdU$^-$ even after injury (96.78 ± 1.15% in control animals vs. 92.81 ± 1.01% in bulbectomized animals) (Fig. S2 *B*–*D*) prompts the suggestion that secretagogin expression is inducible in resident neurons rather than introduced in a new contingent upon injury (Fig. 4 *G* and *G*′ and Fig. S2). This notion is further supported by secretagogin$^+$ neurons being typically DCX$^-$ (Fig. S2 *E*–*G*) and retaining their NeuN$^+$/S100β$^-$ identity (Fig. S2 *H*–*I*″″) upon bulbectomy.

Secretagogin Loss of Function in Mice Reduces Neuroblast Migration. We used secretagogin$^{-/-}$ mice (Fig. S3) to show that the lack of secretagogin expression impacts neuroblast migration: Domain-specific analysis of the RMS revealed that the dorsoventral diameter of the RMS was reduced in secretagogin$^{-/-}$ animals (Fig. 5 *A*–*A*$_1$′) despite the lack of any major phenotypic difference in morphological appearance, destination, or overall DCX content. To explore further if migration defects exist in secretagogin$^{-/-}$ mice, the density of BrdU$^+$ cells in the proximal and distal RMS was analyzed in control animals and after olfactory bulbectomy (Fig. 5*B*). Bulbectomy increased the density of BrdU$^+$ neuroblasts in both secretagogin$^{-/-}$ and wild-type mice (Fig. 5*B*$_1$). Although the proximal RMS region harbored similar densities of newborn cells, irrespective of genotype or surgery (Fig. 5 *B*$_1$–*B*$_3$ and Table S2), the density of BrdU$^+$ neuroblasts increased

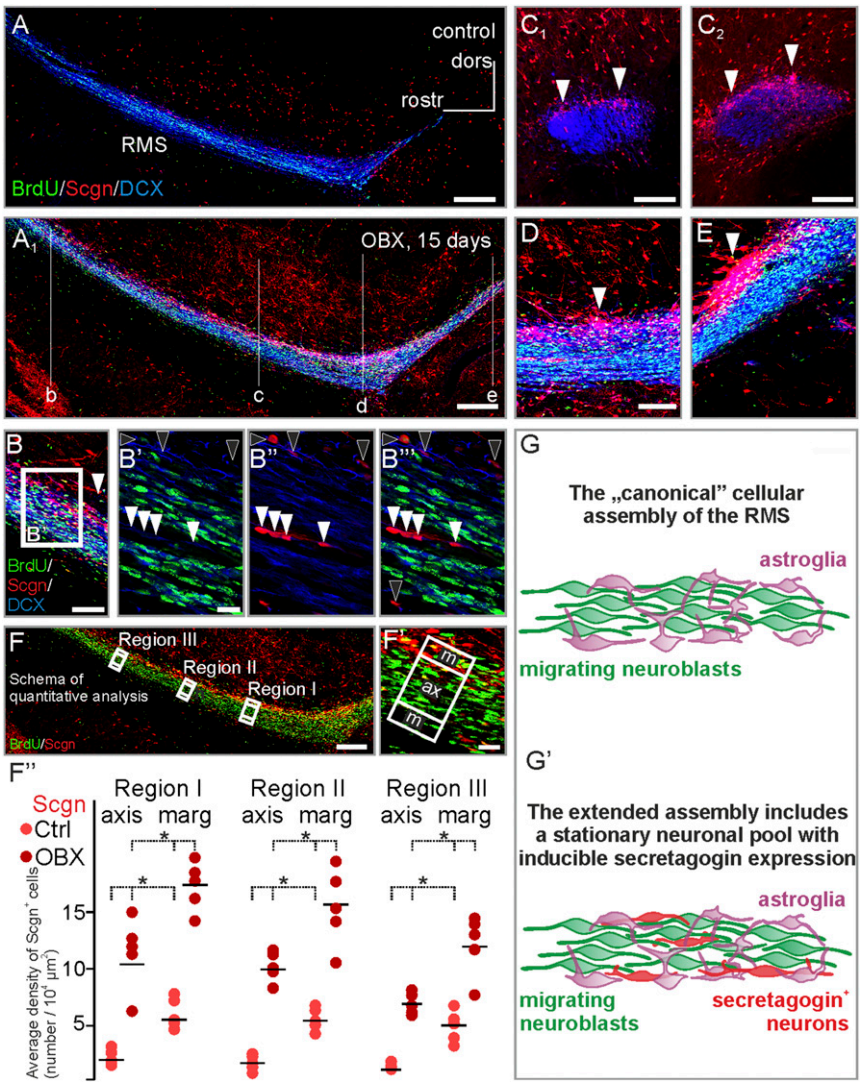

Fig. 4. Unilateral bulbectomy increases the number of secretagogin-expressing cells in the rostral migratory stream. (*A* and *A*$_1$) Secretagogin$^+$ cells not only appeared in the otherwise secretagogin-immunonegative axis of the stream but also typically accumulated in its shell region 15 d after olfactory bulbectomy. Saggital sections are shown in *B*, *D*, and *E*. Coronal sections at the rostrocaudal level indicated in *A*$_1$ are demonstrated in *C*$_1$ and *C*$_2$. (*B*′–*B*‴) Olfactory bulbectomy increased the number of secretagogin$^+$ neurons both in the marginal zone (black arrowheads) and in the axis (white arrowheads) of the RMS. (*F*–*F*″) Fifteen days after bulbectomy, the number of secretagogin-expressing cells increased robustly in the axis and shell domains of the RMS compared with the number of cells detected in sham-operated controls. Secretagogin$^+$ neurons and BrdU$^+$ neuroblasts were counted manually, and their density was calculated in the marginal and axial domains (*F*′) of the distal RMS. To exclude region-specific differences, we carried out identical measurements in three regions of the distal RMS (*F*). The density secretagogin$^+$ neurons increased significantly in both the marginal and axial domains of the RMS. (*G* and *G*′) In addition to astroglia and migrating neuroblasts, the rodent RMS contains secretagogin$^+$ neurons ($P < 0.05$, Student's *t* test). Images in *A*, A1, and *F* were acquired using the tile-and-stitch function. (Scale bars: 300 µm in *A* and *A*$_1$; 200 µm in *F*; 100 µm in *B*, *C*$_1$, *C*$_2$, and *D*; and 10 µm in *B*′ and *F*′.)

significantly only in the distal RMS domains of bulbectomized wild-type mice. In contrast, BrdU$^+$ cell numbers were unchanged in secretagogin$^{-/-}$ mice following surgery (Fig. 5 *B*$_1$–*B*$_3$). This finding suggests that bulbectomy-induced mobilization of neuroblasts toward the injury site is slowed in the absence of secretagogin, implicating secretagogin in a mode of intercellular communication.

Secretagogin Gene Silencing Reduces DCX Expression and Slows Neuroblast Migration. To extend our genetic data on secretagogin's role in modulating neuroblast motility, we injected secretagogin siRNA in close proximity to the "knee region" of the RMS (Fig. 6 *A*–*B*$_1$). Secretagogin immunoreactivity was significantly reduced in and around the injection site, compared with the most distal secretagogin$^+$ somata (Fig. 6*A*$_2$). In parallel, secretagogin silencing abolished immunoreactivity for DCX, an intermediate filament protein involved in neuronal migration (45), around the administration site (Fig. 6 *A*$_1$ and *A*$_{1'}$). DCX loss could not be rescued by olfactory bulbectomy (Fig. S4). The loss of DCX immunoreactivity prompted us to determine the density of BrdU$^+$ cells upstream (toward the ventricle) and downstream (toward the olfactory bulb) from the gene-silencing site (Fig. 6 *B* and *B*$_1$). We observed a decreased density of BrdU$^+$ cells toward the olfactory bulb (Fig. 6 *B*′, *B*$_{1'}$, and *B*$_2$), particularly in the tissue bordering the lesion site (Fig. 6 *B*″ and *B*$_{1''}$). This decrease was paralleled by an increased density of BrdU$^+$ cells upstream (Fig. 6 *B*‴ and *B*$_{1'''}$).

We next extended these in vivo results in vitro using RMS explants from postnatal day (P)5 rats by determining the rate of RMS-derived neuroblast migration into the surrounding embedding medium (Fig. 7*A*). Explants preserved their polarity so that neurons exited the explants exclusively at their rostral (Fig. 7*A*′) but not caudal (Fig. 7*A*″) pole. Secretagogin$^+$ neurons typically accumulated at the margins of the RMS (Fig. 7*A*‴), recapitulating the typical arrangement in vivo (Fig. 1*A*). In control experiments, β-III-tubulin (TUJ1)$^+$ neurons invaded the Matrigel along well-defined streams outlined by secretagogin$^+$ neurons (Fig. 7 *A*$_1$–*A*$_{1''}$), recapitulating in vivo arrangements in both rodents and humans. In contrast, secretagogin knockdown (Fig. 7*A*$_4$) disrupted the migratory pattern of TUJ1$^+$ neurons (Fig. 7 *A*$_2$–*A*$_{2''}$). Notably, the distance covered by migratory secretagogin$^+$ cells decreased significantly (Fig. 7*A*) with a marked reduction in the rate of migrating cells borne at the rostral tip of the explants (Fig. 7 *A*$_3$ and *A*$_5$).

To support the notion that secretagogin$^+$ neurons are critical for neighboring neurons' DCX expression, implying the determination of their motility, we have dissociated the RMS of P5 rats. Neuroblasts were identified by their TUJ1 immunoreactivity (Fig. 7*B*). DCX immunoreactivity in TUJ1$^+$ neurons was typically confined to neurons with in contact with secretagogin$^+$ cells (Fig. 7 *B*–*B*$_{1'}$). In contrast to this even, nonpolarized distribution of cells seeded on poly-D-lysine (PDL) coating, DCX$^+$ RMS neurons on laminin appeared in a string-like arrangement concentrated around spindle-shaped secretagogin$^+$ cells (Fig. 7 *B*$_2$–*B*$_{2''}$). Knockdown of secretagogin expression left overall DCX expression unaltered at the transcriptional level as shown by quantitative PCR (qPCR) (Fig. 7*B*$_3$). This finding suggests that DCX expression is not directly regulated by secretagogin but instead that secretagogin expression regulates cell motility through an extracellular mechanism.

Secretagogin Regulates MMP-2 Release to Reorganize the Extracellular Matrix. Migrating neurons traverse the extracellular matrix, which not only forms a mechanical barrier but also serves to anchor interacting guidance cues (46–48). We hypothesized that secretagogin$^+$ neurons actively shape the surrounding matrix to impact neuroblast migration. To explore this notion, we looked for interacting partners of secretagogin in RMS micropunches (Fig. 8*A*) of control and bulbectomized rats. Secretagogin-interacting proteins were identified in both Ca^{2+}-enriched and Ca^{2+}-free conditions by mass spectrometry (Fig. 8 *B* and *B*$_1$) (35). Among the 264 identified proteins, 64 were considered to be secretagogin-specific in at least one of four conditions (Table S3). Among these, we identified 44 proteins forming secretagogin's Ca^{2+}-dependent interactome, of which 18 were detected in samples from bulbectomized rats. In addition to the actin-bundling protein fascin (49) and the actin dynamic regulator cofilin (50), which reinforce the likely ability of secretagogin$^+$ neurons to undergo morphological changes, we identified annexin V, a protein involved in the release of MMPs, particularly MMP-2 (51). Post hoc Western blotting confirmed the presence of fascin, cofilin, and annexin V in the RMS (Fig. 8*C*), and immunohistochemistry showed these proteins in secretagogin$^+$ cells (Fig. 8 *D*–*D*$_{1''}$ and Fig. S5).

Annexin V's presence in secretagogin$^+$ neurons led us to hypothesize that secretagogin could trigger a secretory pathway to degrade the RMS extracellular matrix (Fig. S6) via regulated MMP-2 release. We first showed that MMP2/9 activity in the RMS is critical for migrating neurons because focal RMS application of Marimastat, a potent and selective MMP-2/MMP-9 inhibitor (52), increased the diameter of the proximal but decreased the diameter of the distal limbs of the RMS (Fig. S7), suggesting migration arrest. Notably, a large number of secretagogin$^+$ neurons accumulated upstream from the drug injection site, especially in the dorsal RMS (Fig. S7*B*). To distinguish MMP-active foci in the RMS, we developed in situ zymography

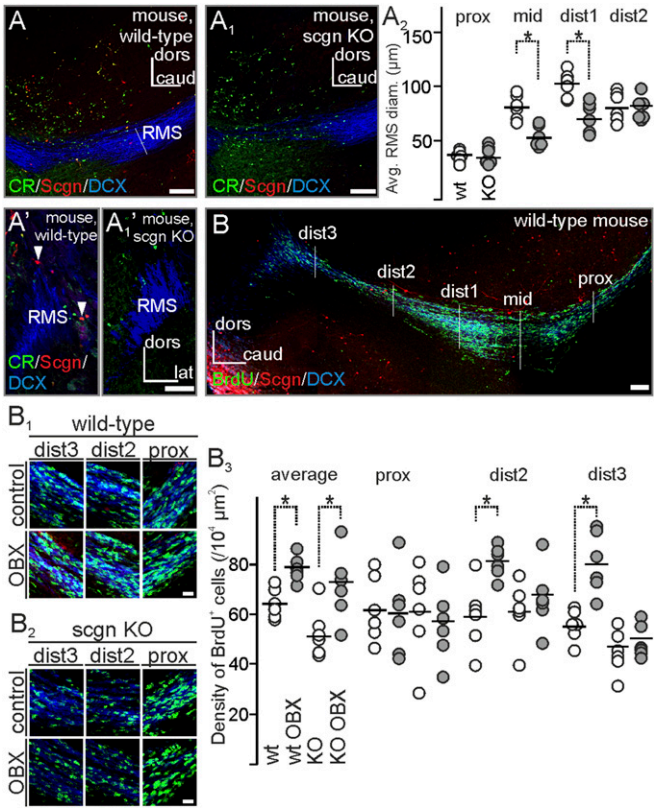

Fig. 5. Altered neuroblast morphology and migration in the RMS of secretagogin$^{-/-}$ mice. (*A*–*A*$_1$) Secretagogin$^{-/-}$ mice lacked any secretagogin expression in their RMS, validating this model. (*A*$_2$) The dorsoventral diameter of the middle and distal domains of the RMS was narrower in secretagogin$^{-/-}$ mice. (*B*–*B*$_3$) Olfactory bulbectomy increased the overall density of BrdU$^+$ neurons in the RMS. No genotype or surgery effects were found in the proximal RMS domain, but olfactory bulbectomy increased the density of BrdU$^+$ cells in the distal RMS regions of wild-type but not secretagogin$^{-/-}$ mice. $P < 0.05$, Student's *t* test. Image in *B* was acquired using the tile-and-stitch function. caud, caudal; CR, calretinin; dist, distal; lat, lateral; prox, proximal. (Scale bars: 100 μm in *A*–*A*$_1$ and *B*; 10 μm for all captures in *B*$_1$ and *B*$_2$.)

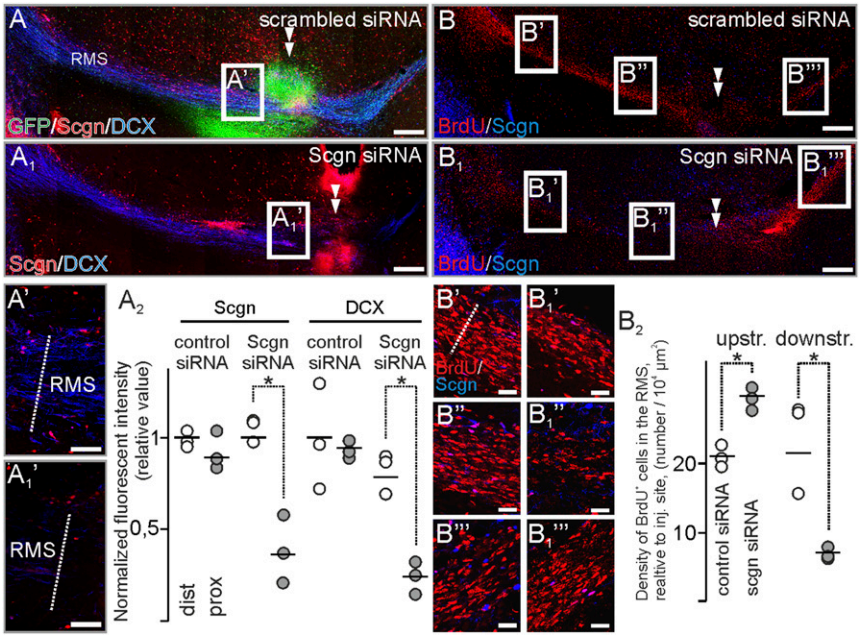

Fig. 6. In vivo secretagogin silencing decreases DCX expression and slows neuroblast migration in the RMS. (*A*–*A*$_2$) Secretagogin (*A*$_1$ and *A*$_{1'}$) but not scrambled siRNA (*A* and *A*′) reduced DCX expression locally (arrowheads in *A* and *A*$_1$). This effect is independent of olfactory bulbectomy (Fig. S4). Note the reduced secretagogin expression upon using specific (*A*$_{1'}$) but not scrambled (*A*′) siRNA and compared with distal RMS free of silencing effect (*A*$_2$). (*B*–*B*$_2$) The density of BrdU$^+$ cells decreased rostral but increased caudal to the silencing site (*B*$_2$). $P < 0.05$, Student's *t* test. Images in *A*, *A*$_1$, *B*, and *B*$_1$ were acquired using the tile-and-stitch function. (Scale bars: 200 µm in *A*, *A*$_1$, *B*, and *B*$_1$; 25 µm in *A*′ and *A*$_{1'}$; 15 µm in *B*′–*B*$_{1'''}$.)

(Fig. S5*D*) and showed gelatinase activity in both axial and marginal regions (Fig. S5*D* and Fig. 8*E*), which harbor the bulk of secretagogin$^+$ neurons (see also Fig. 1*A*). High-resolution orthogonal confocal imaging revealed that MMP-2 foci typically were anchored at the outside surface of secretagogin$^+$ neurons in P5 RMS explants, as is compatible with MMP-2 secretion (Fig. 8 *F* and *F*$_1$). Further support came through gel-zymography in secretagogin$^{-/-}$ mice: The proenzyme form of MMP-2 (proMMP-2) increased in the fraction containing intracellular and membrane-bound enzymes but decreased in the extracellular fraction prepared from RMS micropunches (Fig. 8 *G* and *G*$_1$). We extended this finding by showing that secretagogin silencing increases the level of proMMP-2, but not proMMP-9, in the cytosolic fraction of SH-SY5Y neuroblastoma cells (Fig. 8 *H* and *H*$_1$). Impaired externalization of proMMP-2 likely involved annexin V because annexin V knockdown led to a similar increase of intracellular proMMP-2 (Fig. S5 *E* and *E*$_1$).

Decreased levels of externalized proMMP-2 suggest reduced active MMP-2 extracelluarly. We have measured the protein level of active MMP-2 by Western blotting in RMS micropunches of control and bulbectomized rats. ProMMP-2 and active MMP-2 isoforms were separated by their molecular weights (53). Olfactory bulbectomy significantly increased the level of active MMP-2 but not overall proMMP-2 (Fig. 8 *I* and *I*$_1$) in the RMS. Taken together, our data identify differentiated neurons in the mammalian RMS that express secretagogin to initiate a molecular cascade through annexin V to increase MMP-2 release, thus remodelling the extracellular matrix to aid neuroblast migration (Fig. 8*J*) (15, 16).

Discussion

Researchers have extensively investigated the mechanisms that regulate neuroblast migration in the fetal brain and have identified principal guidance rules in immature tissues. Nevertheless, the RMS of the adult rodent (2) and primate (40) brain is a differently structured, mature anatomical domain that relies on alternative migration cues. Much of our existing knowledge about how newborn cells move in this predominantly glial tube includes glia–neuroblast interactions. Overall, disruption of the glial tunnel as shown in neural cell adhesion molecule- (54) or β1-integrin– (55) deficient mice leads to neuroblast migration defects. In addition to factors related to nonsoluble cell-adhesion (56), astrocytes can use and release soluble signals to orchestrate the movement of RMS neuroblasts (18). At the same time, neuroblasts are proactive in shaping their own journey by relying on physiologically conserved mechanisms, such as Slit/Robo signaling, to clear astrocytic processes (16).

Ca^{2+}-binding proteins are widely used to distinguish and characterize neuronal subsets in the mammalian brain. In addition to parvalbumin, calbindin, and calretinin, secretagogin is a useful marker for identifying forebrain neurons (57). Here we show that the rodent RMS harbors a secretagogin$^+$ neuronal contingent that is non–self-renewing, morphologically differentiated, and may be wired into synaptically connected neuronal circuits.

Secretagogin$^+$ neurons integrated along the total RMS. Thus, secretagogin$^+$ neurons also occurred in the axial RMS domain sent perpendicularly oriented processes to reach the space between neuroblasts and to surround neurites. Secretagogin expression of RMS neurons could be induced by olfactory bulbectomy, suggesting its injury-induced activation to allow for enhanced forward neuroblast migration. Therefore we suggest that a latent neuronal cohort resides in the RMS that will up-regulate its secretagogin content only when pathophysiologically primed to partake in the MMP-2–mediated reorganization of the RMS.

Both insoluble and soluble signals are critically reliant upon the composition and dynamic regulation of the extracellular matrix. Innate components of the matrix can themselves operate as migration signals; for instance, hyaluronan acts on Rhamm receptors expressed on neuroblasts (24). However, the importance of the extracellular domain extends far beyond direct actions between matrix molecules and cell-surface receptors; instead, it offers a critical interface for a wide array of factors and signaling molecules that regulate migration (3–7, 25, 26, 58). Dynamic restructuring of the extracellular matrix is critical in RMS neuroblast migration. Therefore, a coordinated release of endogenous matrix-lytic enzymes, MMPs, can effectively and focally impact intercellular signaling and migration in select pericellular microdomains. We hypothesized that, instead of secreting specific ligands or factors, secretagogin$^+$ neurons regulate neuroblast migration by controlling the reassembly of the extracellular matrix.

In addition to characterizing a hitherto unexplored cell cohort in the RMS, we describe an enzyme externalization mechanism which (*i*) works on an on-demand principle, (*ii*) was known only

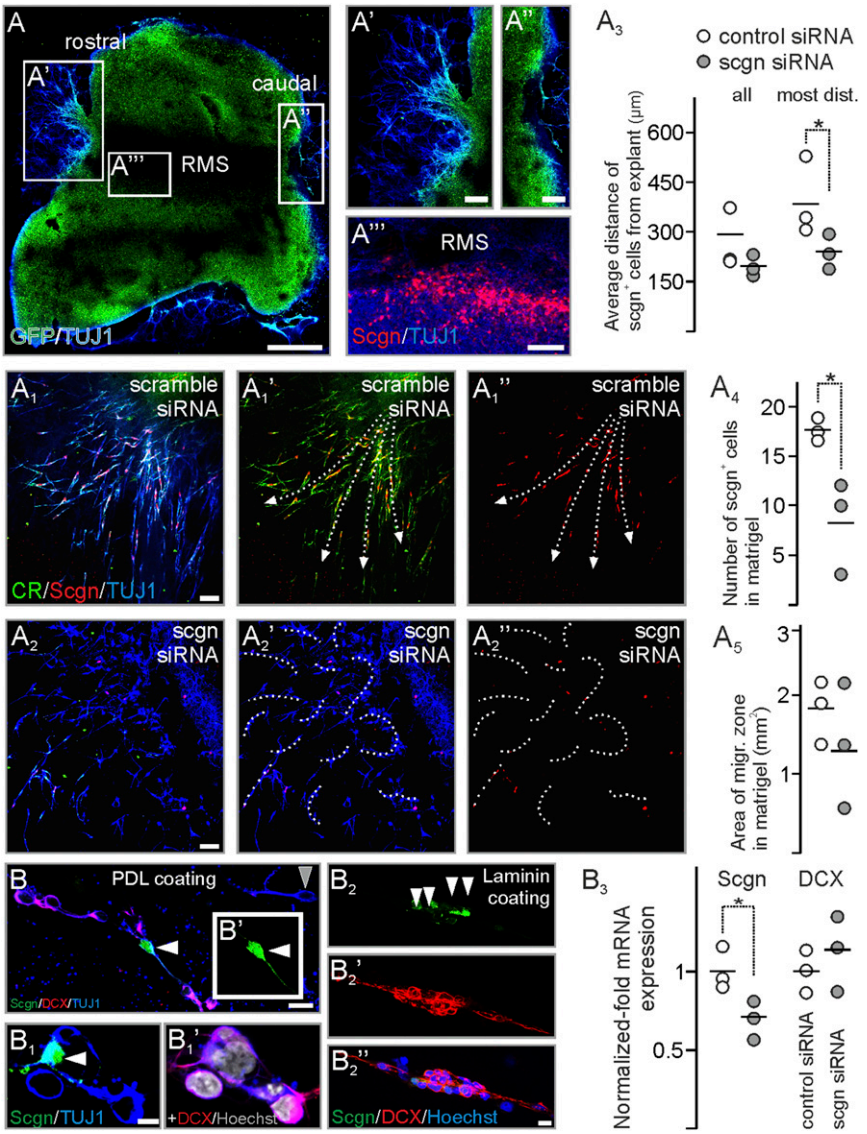

Fig. 7. *Secretagogin silencing disrupts neuroblast migration in vitro. (A–A‴) RMS explants from P5 rat pups preserve polarity with migrating cells at the rostral (A′) but not caudal (A″) pole with secretagogin$^+$ neurons retaining their positions within explants (A‴). (A_1–$A_{2''}$) In controls neuroblasts migrate from the rostral pole of the RMS explants into Matrigel along corridors (arrows in $A_{1'}$ and $A_{1''}$), which are shaped by secretagogin$^+$ neurons. Secretagogin silencing disrupts cell migration (dashed curves in $A_{2'}$ and $A_{2''}$). (A_3–A_5) Although the total area in the Matrigel occupied by migratory neurons decreased only nonsignificantly upon gene silencing, both the maximal and the average distance of secretagogin$^+$ cells was significantly reduced from RMS exit. (B–$B_{1'}$) In primary culture from P5 RMS plated on PDL, neuroblasts contacting secretagogin$^+$ neurons (white arrowheads in B and B_1) typically expressed DCX. (The gray arrowhead in B points to a DCX$^-$ neuron.) (B_2–$B_{2''}$) On laminin-coated surfaces, secretagogin$^+$ neurons (white arrowheads in B_2) formed scaffolds for DCX$^+$ neuroblasts. (B_3) Secretagogin silencing decreased secretagogin mRNA levels but left DCX mRNA expression unaltered. $P < 0.05$, Student's t test. (Scale bars: 500 μm in A; 70 μm in A'–A'''; 25 μm in A_1–$A_{1''}$; 10 μm in B; and 3 μm in $B_{2''}$.)*

in tumor biology but not in focal pericellular mechanisms in the healthy adult, and (*iii*) promotes the migration of the neighboring cells but not the enzyme-releasing cell itself. More than 20 members of the MMP family cleave matrix components. In the developing central nervous system, MMP-2 and MMP-9 attracted much attention when rat postmitotic cerebellar granule neuron precursors (59) and human neuroepithelial stem cells (60) were shown to express MMP-2 and MMP-9–deficient mice showed granule cell migration defects (61). The expression profile of the different MMP members in the postnatal RMS showed the presence of MMP-2, but not MMP-9 (Fig. S6*A*) (12), and migrating neuroblasts were found to express membrane-type MMP 5 (MT5-MMP) (12). Using in situ zymography and immunohistochemistry, we now have identified secretagogin$^+$ neurons as MMP-2–expressing foci. We argue that secretagogin regulates MMP-2 release because (*i*) mass spectrometry identified annexin V, a protein involved in MMP-2 release (51), in secretagogin's interactome; (*ii*) secretagogin$^{-/-}$ RMS showed reduced proMMP-2 release; (*iii*) knockdown of secretagogin or annexin V expression in SH-SY5Y neuroblastoma cells selectively increased the level of intracellular proMMP-2, but not proMMP-9; and (*iv*) active MMP-2 increased in RMS micropunches after bulbectomy. Thus, secretagogin$^+$ neurons can dissemble and rearrange the extracellular matrix to promote the migration of neighboring molecules. Blocking neuroblast migration by MMP inhibition using Marimastat led to increased secretagogin expression in marginal RMS cells upstream of the inhibition site, possibly reflecting a reactive and up-regulated secretagogin-mediated release of MMP activity in these cells to

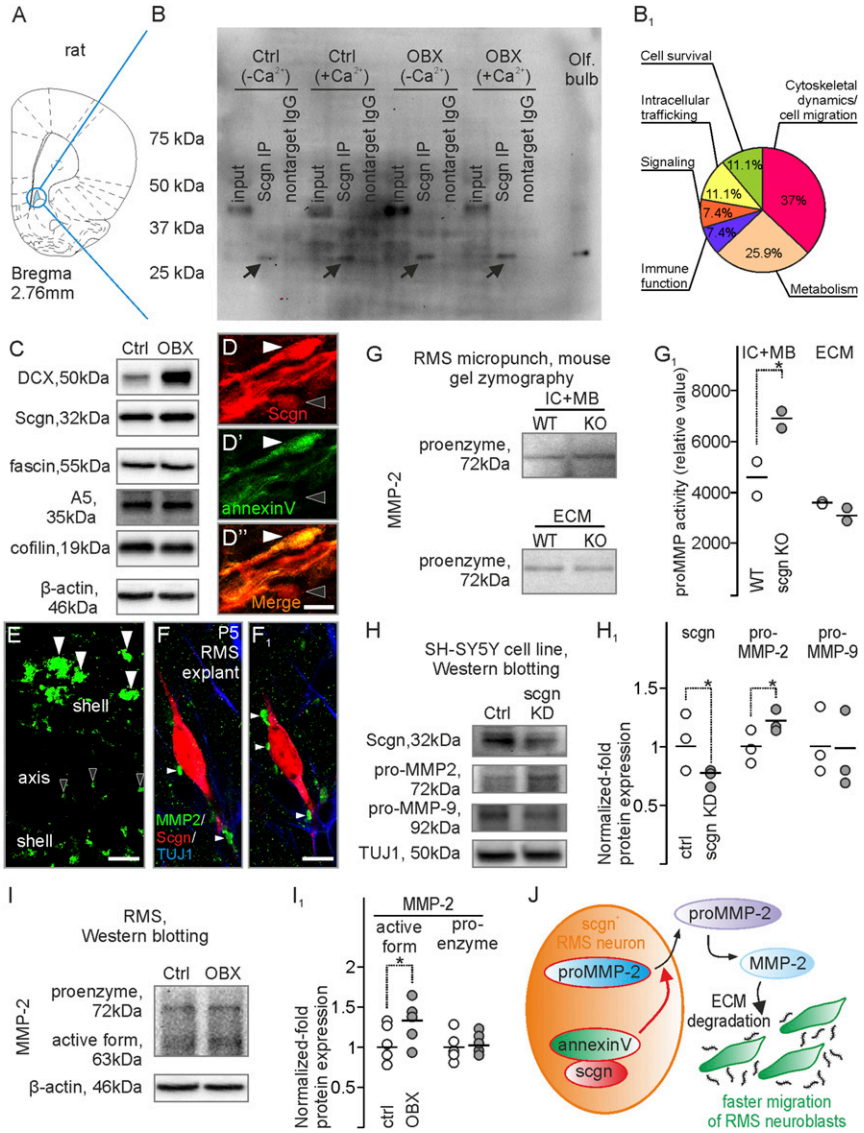

Fig. 8. Secretagogin regulates MMP-2 release. (*A* and *B*) RMS micropunch samples from bulbectomized and control rats were immunoprecipitated with secretagogin in Ca^{2+}-containing or Ca^{2+}-free isolation buffers and were subjected to mass spectrometry. (B_1) Functional distribution of secretagogin-interacting proteins recruited from samples of bulbectomized animals and homogenized in Ca^{2+}-containing isolation buffer. (*C*) Western blotting verified DCX, secretagogin, fascin, annexin V, and cofilin expression in the RMS. (*D*–*D*′′) Post hoc immunohistochemistry resolved annexin V immunoreactivity in secretagogin$^+$ neurons in the RMS (white arrowheads). The black arrowhead points to an annexin V$^-$/secretagogin$^+$ neuron. (*E*) In situ zymography revealed gelatinase activity in the RMS that was reminiscent of the distribution of secretagogin$^+$ neurons. White and black arrowheads indicate profiles in the shell and axial domains of the RMS, respectively. (*F* and F_1) MMP2$^+$ profiles on the extracellular surface of secretagogin$^+$ neurons in RMS explants (serial reconstruction, 700-nm thin optical slices, consecutive z-stack images). (*G* and G_1) Gel zymography from RMS micropunches showed increased proMMP-2 levels in both intracellular and membrane-bound fractions of secretagogin$^{-/-}$ mice, but proMMP-2 levels decreased in the extracellular fraction. (*H* and H_1) Secretagogin silencing increased the expression of the proenzyme form of MMP-2 but not of MMP-9 in SH-SY5Y neuroblastoma cells in vitro. (*I* and I_1) Olfactory bulbectomy increased the level of the active but not of the proenzyme form of MMP-2 in rat RMS. (*J*) Schematic overview of the secretagogin-regulated mechanism in the RMS. Secretagogin regulates the externalization of proMMP-2, thereby limiting the amount of the active form of MMP-2. MMP-2 degrades the extracellular matrix to promote neuroblast migration. $P < 0.05$, Student's *t* test. A5, annexin V; Ctrl, control; OBX, bulbectomized. (Scale bars; 40 μm in *D*; 10 μm in *D*′′ and *E*; and 5 μm in F_1.)

help neuroblast migration. These interactions enable secretagogin-containing neurons to control their own mobility via direct regulation of cytoskeletal proteins. Here, we found that knockdown of secretagogin expression led to reduced mobility of secretagogin$^+$ neurons in RMS explants.

The migration of immature neuronal progeny from the ventricle to the olfactory bulb is a phylogenetically conserved mechanism in mammals (2, 62), including the human infant (1), with a largely similar guidance machinery and cellular expression profiles. Thus, the identification of new cellular components and intercellular signaling mechanisms is paramount to understand the development of the human brain as well as its malfunctions. The adult human subventricular zone principally lacks neural stem cells which could produce tangentially migrating neuroblasts for the olfactory system (1, 63, 64). During infancy, however, corridors of migrating neurons connect the anteroventral tip of the lateral ventricle to the olfactory bulb. This pediatric RMS contains immature neurons that are organized in chains and express DCX (1). Here, we show a continuum of secretagogin$^+$ cells that form corridors from the ventral tip of the lateral ventricle toward and reaching the olfactory trigone. Although neuroblast migration ceases in humans at the early postnatal age (1), we have previously demonstrated that secretagogin$^+$ cells remain present throughout the olfactory tract even in the elderly (37). We suggest that secretagogin$^+$ neurons are critical members of olfactory neuroblast migration in the human fetus, that their dysfunction could play a role in the development of neurological diseases when the olfactory system is compromised, and that, once remobilized, they might be used to for rescue strategies thus providing a tangible starting point for as yet unexplored avenues for redirecting neuroblasts to injury sites.

Materials and Methods

Fetal Tissue. Two male fetal brains with normal development (between gestational weeks 31–33) were selected from the Brain Bank of the Institute of Neurology, Medical University of Vienna, Austria. Fetal brain tissue was obtained from spontaneous or medically induced abortions. Tissues were obtained and used in compliance with the Declaration of Helsinki and following institutional guidelines. The study was performed in the course of a study approved by the Ethical Committee of the Medical University of Vienna (No.104/2009).

Animals, Surgery, and Ethical Approval of Experimental Studies. A total of 65 male rats (Wistar) and 24 male mice were used. Secretagogin-null($^{-/-}$) mice were custom-generated at the Mutant Mouse Resource and Research Center (University of California, Davis, Mouse Biology Program) using the "two-in-one" targeting strategy (65), which generates full knockouts by expressing a termination signal after exon 3 of the secretagogin gene. The ensuing truncated protein therefore terminates before the first EF-hand domain,

excluding Ca^{2+}-binding activity. Food and water were available ad libitum, and animals were kept under standard housing conditions using a 12/12 light/dark cycle. Experimental procedures, including stereotaxic injections and transcardial perfusion, were approved by the Ethical Review Boards of the Semmelweis University and the Medical University of Vienna and conformed to the European Convention for the Protection of Vertebrate Animals used for experimental and other scientific purposes (Protocols: ETS No. 170, ETS No.123, Tierversuchgesetz 2012, BGBI, Nr. 114/2012).

For all rat (n = 33) and mouse (n = 12) surgeries, 6-wk-old animals were used. During surgeries and transcardial perfusions animals were anesthetized i.m. or i.p. with a mixture of ketamine (50 mg/kg body weight) and xylazine (4 mg/kg body weight). After surgery, brains were perfusion-fixed by transcardially applying 4% (wt/vol) paraformaldehyde (PFA) in 0.1 M phosphate buffer (PB). BrdU administration, olfactory bulbectomy, in vivo gene silencing, and in vivo inhibition of matrix MMP activity in rats or transgenic mice are described in *SI Materials and Methods*.

Immunohistochemistry and Imaging. Chromogenic or multiple immunofluorescence histochemistry with select combinations of primary antibodies (Table S4) (1, 34, 35, 49, 51, 66–74) was performed according to published protocols (67). Results of chromogenic histochemistry were captured on an Olympus BX-51 microscope. Sections processed for multiple immunofluorescence histochemistry were inspected and images were acquired on a 780LSM confocal laser-scanning microscope (Zeiss). Procedural details of imaging described in *SI Materials and Methods*.

Electron Microscopy. Sections processed for secretagogin immunohistochemistry (chromogenic detection) were postfixed in buffered 1% OsO_4 at 22–24 °C for 1 h, and were flat-embedded in Durcupan ACM (Fluka). The RMS region was selected and embedded for ultrasectioning. Ultrathin sections (100 nm) were collected on single-slot nickel grids coated with Formvar and were studied on a Jeol 1200 EMX microscope. Primary magnifications ranged from 12,000× to 80,000×, as indicated.

Shotgun Proteomic Analysis. Eluted fractions from secretagogin coimmunoprecipitates were separated on gradient gels (3–12%) and were in-gel digested. Their LC-MS/MS analysis was performed using an an Ultimate 3000 nanoRSLC (Thermo Scientific) coupled to a high-capacity ion trap mass spectrometer (AmaZon ETD; Bruker Daltonics) via a CaptiveSpray ion source (Bruker) (*SI Materials and Methods*) (75–78).

In Situ and Gelatin Zymography. MMP gelatinase activity on sections was detected by in situ zymography (79, 80). Intracellular/cell membrane-bound and extracellular matrix-bound MMP activity was measured using gelatin zymography as previously published (*SI Materials and Methods*) (81, 82).

Cell Migration from RMS Explants. P4/5 rat brains (n = 6) were sectioned sagittally on a vibratome in ice-cold DMEM containing penicillin (100 U/mL) and streptomycin (100 μg/mL) (all from Invitrogen). The RMS was excised and submerged in Matrigel (Corning) in complete culture medium (2 mM Glutamax, B27 supplement in Neurobasal medium) in a 3:1 ratio, which also contained secretagogin or scrambled siRNA (250 pmol/40 μL Matrigel mix) (GE Dharmacon). The explant–Matrigel mix was spread over the surface of Geltrex-coated (Invitrogen) coverslips and incubated in culture medium for 3 d. Coverslips were subsequently immersion-fixed and analyzed by immunocytochemistry (*SI Materials and Methods*).

SH-SY5Y Neuroblastoma and P5 Rat Primary Dissociated RMS Cultures. SH-SY5Y neuroblastoma cells were cultured in DMEM:GlutaMAX containing 5% (vol/vol) FBS, penicillin (100 U/mL) and streptomycin (100 μg/mL) (all from Invitrogen) on PDL-coated coverslips. Using sagittal brain slices, the RMS region was dissected, cells were enzymatically dissociated and plated at a density of 50,000 cells per well on PDL- or laminin-coated coverslips in 24-well plates for morphometry or at a density of 200,000 cells per well in six-well plates for real-time qPCR. Primary neurons and neuroblasts were maintained in DMEM/F12 (1:1) containing B27 supplement [2% (vol/vol)], L-glutamine (2 mM), penicillin (100 U/mL), and streptomycin (100 μg/mL) (all from Invitrogen). In both cultures, secretagogin gene silencing was through the application of secretagogin siRNA (250 pmol/500 μL, diluted in culture medium) (GE Dharmacon) for 2 d. SH-SH-SY5Y cells and primary RMS cultures were subsequently lysed and collected for Western blotting or qPCR, respectively.

Western Blotting. Protein samples from bulbectomized or sham-operated rat (n = 3 per group) RMS were prepared, and their concentrations were determined (83). The protein samples were analyzed under denaturing conditions. Western blotting was performed with the primary antibodies listed in Table S4. Blots were scanned using a Bio-Rad XRS^+ imaging system and were quantified with Image Lab 3.01 (Bio-Rad Laboratories). Protein concentrations were normalized to β-actin (1:10.000) (Sigma).

Real-Time qPCR. qPCR was performed on a Bio-Rad CFX 96 thermal cycler using primer sets listed in Table S5. Samples were run in triplicate to avoid processing-related deviations. Expression levels were normalized to the housekeeping gene encoding GAPDH.

Statistical Analysis. Data were analyzed using Statistica Software Package version 13.2 (StatSoft, Inc.). Pairwise group comparisons in the in vitro histochemical and Western blotting experiments were evaluated using the Student's t test (on independent samples). Data were normalized to controls as indicated. Data were expressed as means ± SEM. A P value of 0.05 was considered statistically significant. In the in vivo experiments, densities of secretagogin$^+$ or BrdU$^+$ cells in the RMS were analyzed by two-factorial ANOVA with genotype (transgenic vs. wild-type) and treatment (bulbectomized vs. control) as between-subjects factors in mice or with treatment (bulbectomized vs. control) and location of cells (marginal vs. axial) as between-subjects factors in rats. Two-factorial ANOVAs in rats were made using square root transformation of data. Post hoc analyses of between-subject effects were performed by Bonferroni's t test. Homogeneity of variance was analyzed by Levene's test. The normality of the sample was examined by Shapiro–Wilk W test. A P value of 0.05 was considered statistically significant.

ACKNOWLEDGMENTS. The excellent technical help of Andrea Németh is gratefully acknowledged. This work was supported by National Brain Research Program of Hungary Grant MTA-SE NAP B, KTIA_NAP_13-2014-0013 (to A.A.); the Swedish Research Council (Vetenskapsrådet) (T.H. and T.G.M.H.); the NovoNordisk Foundation (T.H. and T.G.M.H.); Hjärnfonden (T.H.), European Research Council Grant SECRET-CELLS, 2015-AdG-695136 (to T.H.); and Hungarian Scientific Research Fund Grant NKFI K115422 (to Z.E.T.).

1. Sanai N, et al. (2011) Corridors of migrating neurons in the human brain and their decline during infancy. *Nature* 478(7369):382–386.
2. Lois C, Alvarez-Buylla A (1994) Long-distance neuronal migration in the adult mammalian brain. *Science* 264(5162):1145–1148.
3. Chiaramello S, et al. (2007) BDNF/ TrkB interaction regulates migration of SVZ precursor cells via PI3-K and MAP-K signalling pathways. *Eur J Neurosci* 26(7):1780–1790.
4. Hurtado-Chong A, et al. (2009) IGF-I promotes neuronal migration and positioning in the olfactory bulb and the exit of neuroblasts from the subventricular zone. *Eur J Neurosci* 30(5):742–755.
5. Garzotto D, Giacobini P, Crepaldi T, Fasolo A, De Marchis S (2008) Hepatocyte growth factor regulates migration of olfactory interneuron precursors in the rostral migratory stream through Met-Grb2 coupling. *J Neurosci* 28(23):5901–5909.
6. Paratcha G, Ibáñez CF, Ledda F (2006) GDNF is a chemoattractant factor for neuronal precursor cells in the rostral migratory stream. *Mol Cell Neurosci* 31(3):505–514.
7. Zhou Y, et al. (2015) Regional effects of endocannabinoid, BDNF and FGF receptor signalling on neuroblast motility and guidance along the rostral migratory stream. *Mol Cell Neurosci* 64:32–43.
8. Bagley JA, Belluscio L (2010) Dynamic imaging reveals that brain-derived neurotrophic factor can independently regulate motility and direction of neuroblasts within the rostral migratory stream. *Neuroscience* 169(3):1449–1461.
9. Marks C, Belluscio L, Ibáñez CF (2012) Critical role of GFRα1 in the development and function of the main olfactory system. *J Neurosci* 32(48):17306–17320.
10. Lindberg OR, Persson A, Brederlau A, Shabro A, Kuhn HG (2012) EGF-induced expansion of migratory cells in the rostral migratory stream. *PLoS One* 7(9):e46380.
11. Conover JC, et al. (2000) Disruption of Eph/ephrin signaling affects migration and proliferation in the adult subventricular zone. *Nat Neurosci* 3(11):1091–1097.
12. Bovetti S, Bovolin P, Perroteau I, Puche AC (2007) Subventricular zone-derived neuroblast migration to the olfactory bulb is modulated by matrix remodelling. *Eur J Neurosci* 25(7):2021–2033.
13. Murase S, Cho C, White JM, Horwitz AF (2008) ADAM2 promotes migration of neuroblasts in the rostral migratory stream to the olfactory bulb. *Eur J Neurosci* 27(7):1585–1595.
14. Ono K, Tomasiewicz H, Magnuson T, Rutishauser U (1994) N-CAM mutation inhibits tangential neuronal migration and is phenocopied by enzymatic removal of polysialic acid. *Neuron* 13(3):595–609.
15. Doetsch F, Alvarez-Buylla A (1996) Network of tangential pathways for neuronal migration in adult mammalian brain. *Proc Natl Acad Sci USA* 93(25):14895–14900.
16. Kaneko N, et al. (2010) New neurons clear the path of astrocytic processes for their rapid migration in the adult brain. *Neuron* 67(2):213–223.
17. Peretto P, Merighi A, Fasolo A, Bonfanti L (1997) Glial tubes in the rostral migratory stream of the adult rat. *Brain Res Bull* 42(1):9–21.
18. Mason HA, Ito S, Corfas G (2001) Extracellular signals that regulate the tangential migration of olfactory bulb neuronal precursors: Inducers, inhibitors, and repellents. *J Neurosci* 21(19):7654–7663.

19. Balenci L, et al. (2007) IQGAP1 regulates adult neural progenitors in vivo and vascular endothelial growth factor-triggered neural progenitor migration in vitro. *J Neurosci* 27(17):4716–4724.
20. Bozoyan L, Khlghatyan J, Saghatelyan A (2012) Astrocytes control the development of the migration-promoting vasculature scaffold in the postnatal brain via VEGF signaling. *J Neurosci* 32(5):1687–1704.
21. Platel JC, Dave KA, Bordey A (2008) Control of neuroblast production and migration by converging GABA and glutamate signals in the postnatal forebrain. *J Physiol* 586(16):3739–3743.
22. Bolteus AJ, Bordey A (2004) GABA release and uptake regulate neuronal precursor migration in the postnatal subventricular zone. *J Neurosci* 24(35):7623–7631.
23. Saghatelyan A, de Chevigny A, Schachner M, Lledo PM (2004) Tenascin-R mediates activity-dependent recruitment of neuroblasts in the adult mouse forebrain. *Nat Neurosci* 7(4):347–356.
24. Lindwall C, Olsson M, Osman AM, Kuhn HG, Curtis MA (2013) Selective expression of hyaluronan and receptor for hyaluronan mediated motility (Rhamm) in the adult mouse subventricular zone and rostral migratory stream and in ischemic cortex. *Brain Res* 1503:62–77.
25. Barkho BZ, et al. (2008) Endogenous matrix metalloproteinase (MMP)-3 and MMP-9 promote the differentiation and migration of adult neural progenitor cells in response to chemokines. *Stem Cells* 26(12):3139–3149.
26. Wojcik-Stanaszek L, Gregor A, Zalewska T (2011) Regulation of neurogenesis by extracellular matrix and integrins. *Acta Neurobiol Exp (Warsz)* 71(1):103–112.
27. Yong VW (2005) Metalloproteinases: Mediators of pathology and regeneration in the CNS. *Nat Rev Neurosci* 6(12):931–944.
28. Björklund M, Koivunen E (2005) Gelatinase-mediated migration and invasion of cancer cells. *Biochim Biophys Acta* 1755(1):37–69.
29. Gabelloni P, et al. (2010) Inhibition of metalloproteinases derived from tumours: New insights in the treatment of human glioblastoma. *Neuroscience* 168(2):514–522.
30. Brose N, Petrenko AG, Südhof TC, Jahn R (1992) Synaptotagmin: A calcium sensor on the synaptic vesicle surface. *Science* 256(5059):1021–1025.
31. Südhof TC, Rothman JE (2009) Membrane fusion: Grappling with SNARE and SM proteins. *Science* 323(5913):474–477.
32. Wagner L, et al. (2000) Cloning and expression of secretagogin, a novel neuroendocrine- and pancreatic islet of Langerhans-specific Ca2+-binding protein. *J Biol Chem* 275(32):24740–24751.
33. Mulder J, et al. (2009) Secretagogin is a Ca2+-binding protein specifying subpopulations of telencephalic neurons. *Proc Natl Acad Sci USA* 106(52):22492–22497.
34. Gáti G, Lendvai D, Hökfelt T, Harkany T, Alpár A (2014) Revival of calcium-binding proteins for neuromorphology: Secretagogin typifies distinct cell populations in the avian brain. *Brain Behav Evol* 83(2):82–92.
35. Romanov RA, et al. (2015) A secretagogin locus of the mammalian hypothalamus controls stress hormone release. *EMBO J* 34(1):36–54.
36. Nguyen-Ba-Charvet KT, et al. (2004) Multiple roles for slits in the control of cell migration in the rostral migratory stream. *J Neurosci* 24(6):1497–1506.
37. Attems J, et al. (2012) Clusters of secretagogin-expressing neurons in the aged human olfactory tract lack terminal differentiation. *Proc Natl Acad Sci USA* 109(16): 6259–6264.
38. Jin K, et al. (2004) Proteomic and immunochemical characterization of a role for stathmin in adult neurogenesis. *FASEB J* 18(2):287–299.
39. Blasko J, Fabianova K, Martoncikova M, Sopkova D, Racekova E (2013) Immunohistochemical evidence for the presence of synaptic connections of nitrergic neurons in the rat rostral migratory stream. *Cell Mol Neurobiol* 33(6):753–757.
40. Kornack DR, Rakic P (2001) The generation, migration, and differentiation of olfactory neurons in the adult primate brain. *Proc Natl Acad Sci USA* 98(8):4752–4757.
41. Rakic P (1990) Principles of neural cell migration. *Experientia* 46(9):882–891.
42. Rakic P (2002) Neurogenesis in adult primates. *Prog Brain Res* 138:3–14.
43. Kirschenbaum B, Doetsch F, Lois C, Alvarez-Buylla A (1999) Adult subventricular zone neuronal precursors continue to proliferate and migrate in the absence of the olfactory bulb. *J Neurosci* 19(6):2171–2180.
44. Doetsch F (2003) A niche for adult neural stem cells. *Curr Opin Genet Dev* 13(5): 543–550.
45. des Portes V, et al. (1998) A novel CNS gene required for neuronal migration and involved in X-linked subcortical laminar heterotopia and lissencephaly syndrome. *Cell* 92(1):51–61.
46. de Chevigny A, et al. (2006) Delayed onset of odor detection in neonatal mice lacking tenascin-C. *Mol Cell Neurosci* 32(1-2):174–186.
47. Mobley AK, McCarty JH (2011) β8 integrin is essential for neuroblast migration in the rostral migratory stream. *Glia* 59(11):1579–1587.
48. Curtis MA, et al. (2007) Human neuroblasts migrate to the olfactory bulb via a lateral ventricular extension. *Science* 315(5816):1243–1249.
49. Sonego M, et al. (2013) Fascin regulates the migration of subventricular zone-derived neuroblasts in the postnatal brain. *J Neurosci* 33(30):12171–12185.
50. Alberti S, et al. (2005) Neuronal migration in the murine rostral migratory stream requires serum response factor. *Proc Natl Acad Sci USA* 102(17):6148–6153.
51. Wu L, et al. (2014) Annexin A5 promotes invasion and chemoresistance to temozolomide in glioblastoma multiforme cells. *Tumour Biol* 35(12):12327–12337.
52. Drummond AH, et al. (1999) Preclinical and clinical studies of MMP inhibitors in cancer. *Ann N Y Acad Sci* 878:228–235.
53. Shimokawa Ki K, et al. (2002) Matrix metalloproteinase (MMP)-2 and MMP-9 activities in human seminal plasma. *Mol Hum Reprod* 8(1):32–36.
54. Chazal G, Durbec P, Jankovski A, Rougon G, Cremer H (2000) Consequences of neural cell adhesion molecule deficiency on cell migration in the rostral migratory stream of the mouse. *J Neurosci* 20(4):1446–1457.
55. Belvindrah R, Hankel S, Walker J, Patton BL, Müller U (2007) Beta1 integrins control the formation of cell chains in the adult rostral migratory stream. *J Neurosci* 27(10): 2704–2717.
56. García-Marqués J, De Carlos JA, Greer CA, López-Mascaraque L (2010) Different astroglia permissivity controls the migration of olfactory bulb interneuron precursors. *Glia* 58(2):218–230.
57. Alpár A, Attems J, Mulder J, Hökfelt T, Harkany T (2012) The renaissance of Ca2+-binding proteins in the nervous system: Secretagogin takes center stage. *Cell Signal* 24(2):378–387.
58. Oudin MJ, et al. (2011) Endocannabinoids regulate the migration of subventricular zone-derived neuroblasts in the postnatal brain. *J Neurosci* 31(11):4000–4011.
59. Szklarczyk A, Lapinska J, Rylski M, McKay RD, Kaczmarek L (2002) Matrix metalloproteinase-9 undergoes expression and activation during dendritic remodeling in adult hippocampus. *J Neurosci* 22(3):920–930.
60. Frölichsthal-Schoeller P, et al. (1999) Expression and modulation of matrix metalloproteinase-2 and tissue inhibitors of metalloproteinases in human embryonic CNS stem cells. *Neuroreport* 10(2):345–351.
61. Vaillant C, Didier-Bazès M, Hutter A, Belin MF, Thomasset N (1999) Spatiotemporal expression patterns of metalloproteinases and their inhibitors in the postnatal developing rat cerebellum. *J Neurosci* 19(12):4994–5004.
62. Paredes MF, Sorrells SF, Garcia-Verdugo JM, Alvarez-Buylla A (2016) Brain size and limits to adult neurogenesis. *J Comp Neurol* 524(3):646–664.
63. Arellano JI, Rakic P (2011) Neuroscience: Gone with the wean. *Nature* 478(7369): 333–334.
64. Bergmann O, et al. (2012) The age of olfactory bulb neurons in humans. *Neuron* 74(4): 634–639.
65. Skarnes WC, et al. (2011) A conditional knockout resource for the genome-wide study of mouse gene function. *Nature* 474(7351):337–342.
66. Alpár A, et al. (2010) Slow age-dependent decline of doublecortin expression and BrdU labeling in the forebrain from lesser hedgehog tenrecs. *Brain Res* 1330:9–19.
67. Lendvai D, et al. (2013) Neurochemical mapping of the human hippocampus reveals perisynaptic matrix around functional synapses in Alzheimer's disease. *Acta Neuropathol* 125(2):215–229.
68. Schwaller B, Buchwald P, Blümcke I, Celio MR, Hunziker W (1993) Characterization of a polyclonal antiserum against the purified human recombinant calcium binding protein calretinin. *Cell Calcium* 14(9):639–648.
69. Moriyama K, Yahara I (1999) Two activities of cofilin, severing and accelerating directional depolymerization of actin filaments, are affected differentially by mutations around the actin-binding helix. *EMBO J* 18(23):6752–6761.
70. Nico B, et al. (2006) Increased matrix-metalloproteinase-2 and matrix-metalloproteinase-9 expression in the brain of dystrophic mdx mouse. *Neuroscience* 140(3): 835–848.
71. Mullen RJ, Buck CR, Smith AM (1992) NeuN, a neuronal specific nuclear protein in vertebrates. *Development* 116(1):201–211.
72. Levine JM, Card JP (1987) Light and electron microscopic localization of a cell surface antigen (NG2) in the rat cerebellum: Association with smooth protoplasmic astrocytes. *J Neurosci* 7(9):2711–2720.
73. Shashoua VE, Hesse GW, Moore BW (1984) Proteins of the brain extracellular fluid: Evidence for release of S-100 protein. *J Neurochem* 42(6):1536–1541.
74. Tortoriello G, et al. (2014) Miswiring the brain: Δ9-tetrahydrocannabinol disrupts cortical development by inducing an SCG10/stathmin-2 degradation pathway. *EMBO J* 33(7):668–685.
75. Ghafari M, et al. (2017) Formation of GABA receptor complexes containing alpha1 and alpha5 subunits is paralleling a multiple T-maze learning task in mice. *Brain Struct Funct* 222(1):549–561.
76. Zhang MD, et al. (2016) Comparative anatomical distribution of neuronal calcium-binding protein (NECAB) 1 and -2 in rodent and human spinal cord. *Brain Struct Funct* 221(7):3803–23.
77. Keller A, Nesvizhskii AI, Kolker E, Aebersold R (2002) Empirical statistical model to estimate the accuracy of peptide identifications made by MS/MS and database search. *Anal Chem* 74(20):5383–5392.
78. Nesvizhskii AI, Keller A, Kolker E, Aebersold R (2003) A statistical model for identifying proteins by tandem mass spectrometry. *Anal Chem* 75(17):4646–4658.
79. Oh LY, et al. (1999) Matrix metalloproteinase-9/gelatinase B is required for process outgrowth by oligodendrocytes. *J Neurosci* 19(19):8464–8475.
80. Okabe M, Nyakas C, Buwalda B, Luiten PG (1993) In situ blotting: A novel method for direct transfer of native proteins from sectioned tissue to blotting membrane: Procedure and some applications. *J Histochem Cytochem* 41(6):927–934.
81. Papp AM, et al. (2007) Visible light induces matrix metalloproteinase-9 expression in rat eye. *J Neurochem* 103(6):2224–2233.
82. Hattori S, Fujisaki H, Kiriyama T, Yokoyama T, Irie S (2002) Real-time zymography and reverse zymography: A method for detecting activities of matrix metalloproteinases and their inhibitors using FITC-labeled collagen and casein as substrates. *Anal Biochem* 301(1):27–34.
83. Bradford MM (1976) A rapid and sensitive method for the quantitation of microgram quantities of protein utilizing the principle of protein-dye binding. *Anal Biochem* 72: 248–254.